Eur. Phys. J. D **20**, 133–148 (2002)
DOI: 10.1140/epjd/e2002-00107-2

THE EUROPEAN PHYSICAL JOURNAL D

Spontaneous emission of an atom placed near a prolate nanospheroid

V.V. Klimov[1], M. Ducloy[2,a], and V.S. Letokhov[3]

[1] P.N. Lebedev Physical Institute, Russian Academy of Sciences, 53 Leninsky Prospect, Moscow 117924, Russia
[2] Laboratoire de Physique des Lasers[b], Université Paris-Nord, Institut Galilée, avenue J.-B. Clément, 93430 Villetaneuse, France
[3] Institute of Spectroscopy, Russian Academy of Sciences, Troitsk 142092, Moscow Region, Russia

Received 2 January 2002 and Received in final form 3 April 2002
Published online 28 June 2002 –

Abstract. The frequency shift and linewidth variation of an atomic oscillator placed next to a prolate dielectric or metal spheroid are found within the framework of the classical approach. Both the frequency shift and linewidth are shown to be substantially dependent on the location of the atom and the form of the nanospheroid and capable of reaching very high values near the surface of the nanospheroid under plasmon (polariton) resonance conditions. The predictions are compared with those found for spherical and cylindrical geometries. The prolate spheroid is treated as a model of a needle tip in apertureless optical scanning microscopy. Effects of sharpness of interaction between the nanospheroid tip and atoms are considered.

PACS. 42.50.-p Quantum optics – 34.50.Dy Interactions of atoms and molecules with surfaces; photon and electron emission; neutralization of ions – 78.67.-n Optical properties of nanoscale materials and structures

1 Introduction

Nanooptics, *i.e.*, optics on a space scale (in one-, two-, or three-dimensional space) much smaller than the optical wavelength λ is a promising avenue of inquiry in nanoscience and technology. Investigations in the field of nanooptics can be arbitrarily subdivided into three interrelated areas:

(1) localization of light on a nanoscale with a view to attaining an ultrahigh spatial resolution (microscopy, optical memory etc.), specifically in near-field optics [1,2];
(2) localization of atoms on a nanoscale by means of light (atom nanooptics [2–4]);
(3) variation of the spectral characteristics of quantum-mechanical systems (atoms, molecules, ions) inside and in the vicinity of nanobodies.

The roots of the latter line of investigation probably lie in the work of Purcell [5], who was the first to discuss the change of the spontaneous emission probability of an atom placed inside a resonator. This question was later studied in detail in works using micro-cavities and came to be known as Cavity QED [6,7]. Within the framework of this line, they analyzed radiation processes in the neighborhood of a wide variety of material bodies whose dimensions are larger than or comparable with the radiation wavelength. A number of works in the literature have been devoted to the studies of the spectroscopic characteristics of an excited atom near a plane interface [8–12].

The spectroscopy of an atom placed both inside and outside a dielectric sphere was considered in [13–16]. In that case, there can occur substantial changes in the spectroscopic properties, because resonance modes (whispering gallery modes [17–19]) can be excited in such spheres. The influence of ideally conducting and dielectric cylinders on the radiation properties of an atom was examined in [20–23]. The cone geometry was considered in [24]. In all these works, the primary emphasis was on the case where the size of the considered body was large in comparison with the radiation wavelength.

However, the spectroscopic properties of atoms also vary greatly in the case of *nanobodies*, *i.e.*, bodies of size much smaller than the radiation wavelength λ. In that case, no resonance modes similar to whispering gallery modes are excited, and the effect of the nanobodies is due to entirely different factors.

First of all, one should note the effect of the surface curvature giving rise to large field gradients. For example, it was demonstrated in [25] that when the diameter of the dielectric nanosphere is very small ($2a \ll \lambda$) the probability of quadrupole transitions (which are due to field gradients) rises in the ratio $(\lambda/a)^2$ (see discussion

[a] e-mail: ducloy@galilee.univ-paris13.fr
[b] UMR 7538 du CNRS

in [26]) compared to that in the case of free space. The same enhancement of quadrupole transitions also occurs in the case of cylindrical geometry [23].

Secondly, in metal nanobodies, 3-D plasmon (polariton) resonances can be excited, which substantially increase transition probabilities. For example, in the case of ideally conducting nanocylinder, the dipole transition probability grows higher in the ratio $(\lambda/a)^2$ [23]. In the case of plasmon resonance in a sphere, there can occur a transition increase of the order of $(\lambda/a)^4$ [27]. It is quite possible that the enormous fluorescence enhancement observed in [28] to take place in the presence of golden nanorods was also associated with the excitation of plasmon resonances.

Therefore, the question naturally arises as to the consideration of the spontaneous emission of an atom in the vicinity of a prolate nanospheroid (dielectric or metallic). First, this case is intermediary between the ideal cases of nanosphere [15,16] and nanocylinder [23]. Secondly, the sharp tip of such a prolate nanospheroid is a natural simple model of the needle tip used in scanning aperture-less microscopy [1] whose interferometric version is capable of ensuring a spatial resolution as high as 1 nm [29]. This is also important in scanning near-field resonance energy transfer (FRET) microscopy using an active probe (exciton-type [30], or fixed excited-atom-type [31]). All these considerations are important motivations for the present work.

Here we consider, within the framework of the perturbation approach, the spectroscopic characteristics of a classical oscillator located outside of a prolate dielectric or metallic nanospheroid. It is well-known that the classical analysis in this case yields the same results as the quantum-mechanical one [32]. The analytical solution of the Maxwell equations for a dipole placed on the axis of an ideally conducting spheroid is well-known [33]. However, the analysis of this solution is rather complicated because of the presence of spheroidal functions. The case of dielectric spheroid is even more complicated. At present, the only known solution is that of the problem of plane-wave diffraction by a dielectric spheroid [34,35]. As far as we know, the analytical solution of the problem of atomic emission near a dielectric spheroid still remains to be found. In this connection, to obtain demonstrative analytical results, we restrict ourselves to the case of prolate nanospheroid. The name nanospheroid is used here in reference to any spheroid with a characteristic size much smaller than the radiation wavelength. We also assume that the distance between the atom and the nanospheroid is much less than the radiation wavelength and that the permittivity of a nanospheroid is independent of frequency (ideal dielectric). Such an approach is of importance from the experimental point of view and allows us to obtain demonstrative analytical results.

The structure of the rest of the paper is as follows. In Section 2 we present general expressions for the variation of the decay rate and frequency shift of an atom placed near any body and simplify them for the case of nanobodies, where one can use quasistatic approximations.

In Section 3, the quasistatic fields near a prolate nanospheroid are derived. Using these fields, we find general expressions for the decay rates and frequency shifts of an atom placed near a nanospheroid. In Section 4, we analyze the results obtained in Section 3 for the decay rates and compare them with those occurring near a sphere and a cylinder. In this section, we also apply the atom–nanospheroid system to simulate the operation of an aperture-less scanning microscope. And finally in Section 5, we analyze the frequency shifts of a dipole in the vicinity of a dielectric and a metal nanospheroid.

2 Linewidth and frequency shift of an atomic oscillator in the presence of an arbitrary body

So, let us consider a linear (1-D) oscillator located in vacuum at the point $\mathbf{r}'$ near an arbitrary body, having a permittivity ε. In the classical approach, the change in the emission characteristics is associated with the radiation reaction [36]. If the atom is treated as a nonrelativistic oscillator consisting of a stationary charge $-e$ and a charge e oscillating about it, the equation of motion of the latter in the absence of any body has the form

$$m\delta\ddot{\mathbf{r}} = \frac{2e^2}{3c^3}\delta\dddot{\mathbf{r}} - m\omega_0^2\delta\mathbf{r} \tag{1}$$

or, in the case of weak radiation reaction,

$$m\delta\ddot{\mathbf{r}} + m\gamma_0\delta\dot{\mathbf{r}} + m\omega_0^2\delta\mathbf{r} = 0. \tag{2}$$

Here $\delta\mathbf{r}$ is the radius vector of the oscillating charge, measured from stationary charge, ω_0 is the frequency of free oscillations, and

$$\gamma_0 = \frac{2e^2}{3c^3}\frac{\omega_0^2}{m} \tag{3}$$

is the total linewidth in vacuum, m is the electron mass, and $\mathbf{c}$ is the velocity of light in vacuum.

If the oscillator is located at the point $\mathbf{r}'$ in the vicinity of a body, it is acted upon by an additional reflected field $\mathbf{E}^{(\mathrm{R})}(\mathbf{r}')$, so that its equation of motion takes the form

$$\begin{aligned} m\delta\ddot{\mathbf{r}} + m\gamma_0\delta\dot{\mathbf{r}} + m\omega_0^2\delta\mathbf{r} &= e\mathbf{E}^{(\mathrm{R})}(\mathbf{r}'+\delta\mathbf{r},t) \approx e\mathbf{E}^{(\mathrm{R})}(\mathbf{r}',t) \\ m\ddot{\mathbf{d}} + m\gamma_0\dot{\mathbf{d}} + m\omega_0^2\mathbf{d} &= e^2\mathbf{E}^{(\mathrm{R})}(\mathbf{r}',t) \end{aligned} \tag{4}$$

where $\mathbf{d} = e\delta\mathbf{r}$ is the electric dipole momentum of the atomic transition. Projecting this equation onto the oscillation direction, we get:

$$m\ddot{d} + m\gamma_0\dot{d} + m\omega_0^2 d = e^2\frac{\mathbf{d}_0\mathbf{E}^{(\mathrm{R})}(\mathbf{r}',t)}{d_0} \tag{5}$$

where $\mathbf{d}_0$ is the dipole oscillation vector amplitude.

Assuming that all the quantities involved are proportional to $\exp(-\mathrm{i}\omega t)$, we obtain the dispersion equation defining the line characteristics in the presence of the body:

$$\omega^2 + \mathrm{i}\omega\gamma_0 - \omega_0^2 + \frac{e^2}{md_0^2}\mathbf{d}_0\mathbf{E}^{(\mathrm{R})}(\mathbf{r}',\omega) = 0. \tag{6}$$

When the corrections to the free-space oscillation frequency and oscillator linewidth are small in comparison with the characteristic frequency scale, the solution of this equation may be obtained in a perturbative approach:

$$\omega = \omega_0 - \frac{\mathrm{i}}{2}\gamma_0 - \frac{e^2}{2m\omega_0}\frac{\mathbf{d}_0\mathbf{E}^{(\mathrm{R})}(\mathbf{r}',\omega_0)}{d_0^2}\,. \tag{7}$$

Separating the real and imaginary parts of this expression and using expression (3) for the linewidth in the vacuum free space, we obtain in this approximation the following formula for the linewidth change (see, for example, [6,36]):

$$\frac{\gamma}{\gamma_0} = 1 + \frac{3}{2}\mathrm{Im}\frac{\mathbf{d}_0\mathbf{E}^{(\mathrm{R})}(\mathbf{r}',\omega_0)}{d_0^2k_0^3} \tag{8}$$

and for the frequency shift:

$$\frac{\omega-\omega_0}{\gamma_0} = -\frac{3}{4}\mathrm{Re}\frac{\mathbf{d}_0\mathbf{E}^{(\mathrm{R})}(\mathbf{r}',\omega_0)}{d_0^2k_0^3}\,. \tag{9}$$

Here and elsewhere, $k_0 = \omega_0/c$ and $k = \omega/c$ stand for the wave vectors in free space.

So, to obtain concrete results, it is sufficient to calculate the reflected field $\mathbf{d}_0\mathbf{E}^{(\mathrm{R})}(\mathbf{r}',\omega)$ at the location of the atom. The reflected field is determined by solving the Maxwell equation with the dipole source. It is also possible to calculate the radiative linewidth in a direct way. To do so, one should calculate the energy flow from the oscillator to infinity and normalize it to the energy flow from the free oscillator:

$$\frac{\gamma}{\gamma_0} = \frac{\int\left|\left(\mathbf{E}^{(0)}+\mathbf{E}^{(\mathrm{R})}\right)\times\left(\mathbf{H}^{(0)}+\mathbf{H}^{(\mathrm{R})}\right)\right|^2_{r\to\infty}\mathrm{d}\Omega}{\int\left|\left(\mathbf{E}^{(0)}\right)\times\left(\mathbf{H}^{(0)}\right)\right|^2_{r\to\infty}\mathrm{d}\Omega}\,. \tag{10}$$

The classical expressions (8, 9) are valid for any body permittivities, including complex ones. In the case of real permittivity, one can show the equivalence of the classical and quantum-mechanical perturbation approaches for the decay rates [6,7,32]. Using the recent approaches to the quantization of electromagnetic fields in media with losses and dispersion, one can also show the equivalence of classical and quantum-mechanical perturbation approaches in the case of complex permittivity [37,38].

Expressions (8, 9) are useful where the solution of the classical dipole emission problem is known. In our case, no such solution is known. However, in the case of bodies (nanobodies) whose size is small in comparison with the radiation wavelength, it possible to build the perturbation theory in terms of the wave vector $\mathbf{k}$ [39], or, more exactly, in terms of the ratio between the characteristic size a of the body and the wavelength λ, *i.e.*, $ka \ll 1$.

In this case, it is possible to expand the expression for the reflected field $\mathbf{d}_0\mathbf{E}^{(\mathrm{R})}(\mathbf{r}',\omega)$ governing both the frequency shift and the change of the decay rate in a power series of k:

$$\frac{\mathbf{d}_0\mathbf{E}^{(\mathrm{R})}(\mathbf{r}',\omega_0)}{d_0^2} = a_1 + b_1k + c_1k^2 + \mathrm{i}d_1k^3 + ... \tag{11}$$

where the coefficients a_1, b_1, c_1, and d_1 are determined by solving some quasistatic problems [39].

It is important to note that the first three terms are due to near fields, while radiation fields appear only starting with the fourth term, which is proportional to k^3.

In the case of loss-free nanobody, the coefficients a_1, b_1, c_1, and d_1 appear to be real, and the expressions for the frequency shift and decay rate variations have the following form for $k > 0$:

$$\frac{\gamma}{\gamma_0} = 1 + \frac{3}{2}d_1 + ... \tag{12}$$

$$\frac{\omega-\omega_0}{\gamma_0} = -\frac{3}{4}\frac{a_1 + b_1k + c_1k^2}{k^3} + ... \tag{13}$$

To find concrete expressions for the coefficients a_1, b_1, c_1, and d_1, one should solve a sequence of quasistatic problems. The coefficient a_1 is determined by solving the static problem on the dipole near the nanobody. This allows us to find the leading term of frequency shift (13). The rest of the coefficients are determined by solving more complicated quasistatic problems. However, to find the coefficient d_1 describing radiative decay rate (12), one can use expression (10).

In the case of nanobodies of interest to us, radiation is a dipole-type, and so expression (10) reduces to the ratio between the square of the total dipole momentum and the square of the dipole momentum of the atomic oscillator:

$$\frac{\gamma}{\gamma_0} = \frac{|\mathbf{d}_{\mathrm{tot}}|^2}{|\mathbf{d}_0|^2}\,. \tag{14}$$

Here $\mathbf{d}_{\mathrm{tot}}$ is the total dipole momentum of the atom + nanobody system. By comparing between expressions (12, 14), one can easily find the following expression for the coefficient d_1:

$$d_1 = \frac{2}{3}\left(\frac{|\mathbf{d}_{\mathrm{tot}}|^2}{|\mathbf{d}_0|^2} - 1\right). \tag{15}$$

So, to describe the decay rate and frequency shift variations occurring in the presence of any nanobody, it is sufficient to solve the static problem on a dipole near the nanobody. The total dipole momentum thus found will allow one to find, according to (14), the decay rate, while the reflected field will make it possible to find, according to (13), the frequency shift.

In the case of medium with losses, all of the coefficients a_1, b_1, c_1, and d_1 are complex. This fact causes no qualitative changes in the frequency shift, but the decay rate changes substantially. In this case, the decay rate is governed by all its first terms, rather than the fourth term d_1 in expression (11):

$$\frac{\gamma}{\gamma_0} = 1 + \frac{3}{2}\mathrm{Im}\left(\frac{a_1}{k^3} + ...\right) + \frac{3}{2}\mathrm{Re}(d_1) + ... \tag{16}$$

$$\frac{\omega-\omega_0}{\gamma_0} = -\frac{3}{4}\mathrm{Re}\left(\frac{a_1}{k^3} + ...\right). \tag{17}$$

Such a change in the decay rate has a simple physical explanation. In the case of medium with losses, the energy of the oscillator is emitted into the outer space,

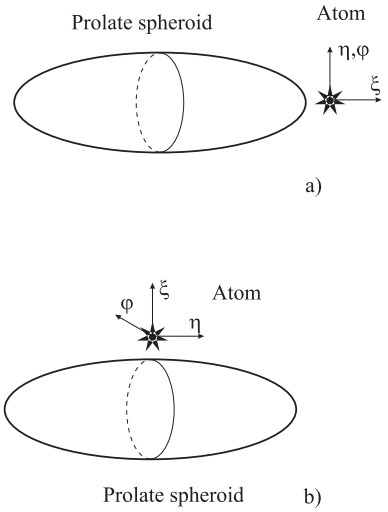

Fig. 1. Geometry of the problem: (a) atom near the vertex of the nanospheroid; (b) atom near the equator of the nanospheroid. The arrows show the possible orientations of the dipole momentum of an atom along the coordinate lines of the prolate spheroid coordinate system.

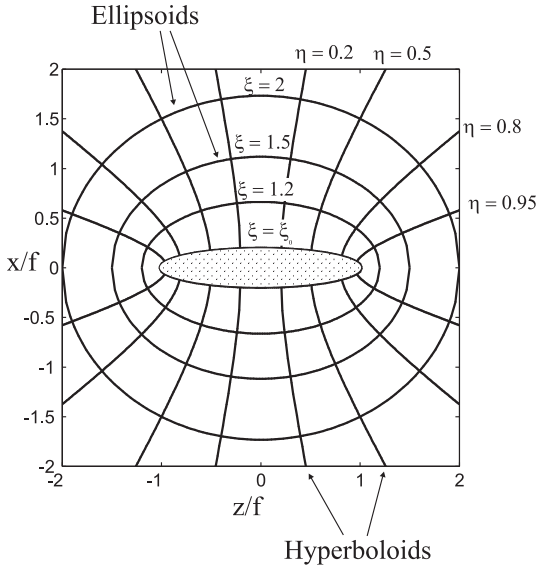

Fig. 2. Coordinate system of a prolate spheroid. Hachure indicates the nanospheroid under consideration ($\xi = \xi_0$).

as well as *dissipated into the nanobody*. Let us stress that expression (16) for the decay rate describes all the losses of energy, while the rate of radiative losses is described by

$$\frac{\gamma}{\gamma_0} = \frac{|\mathbf{d}_{\rm tot}|^2}{|\mathbf{d}_0|^2} = \left|1 + \frac{3}{2} d_1\right| \tag{18}$$

in any case.

In the present paper, we calculate the leading terms for the frequency shift (a_1) and for the decay rate variation (a_1, d_1) in the presence of a prolate spheroid with a complex permittivity. The geometry of the problem is presented in Figure 1.

3 An atom near a prolate nanospheroid

In this section, we will consider the case of a prolate spheroid whose size is small in comparison with the radiation wavelength. We assume also that the atom is located in close vicinity of the nanospheroid. The geometry of the problem is presented in Figure 1. According to Section 2 (Eqs. (17, 18)), the decay rate can in that case be found from the total dipole momentum and the frequency shift from the reflected field.

3.1 Solution of the quasistationary problem

To find the total dipole momentum and the reflected field, one should solve the classical quasistatic problem

$$\begin{aligned} {\rm rot}\mathbf{E} &= 0 \\ {\rm div}\mathbf{D} &= 4\pi\rho \end{aligned} \tag{19}$$

where the charge density is defined by the usual expression

$$\rho = -\left(\mathbf{d}_0\nabla'\right)\delta^{(3)}\left(\mathbf{r}-\mathbf{r}'\right)\mathrm{e}^{-\mathrm{i}\omega t} \tag{20}$$

where δ is the three-dimensional Dirac delta function and ∇' means gradient over radius vector of the atom, $\mathbf{r}'$.

Hereafter we will omit the time dependence of the fields. Introducing the potential $\tilde{\varphi}$

$$\mathbf{E} = -\nabla(\mathbf{d}_0\nabla')\tilde{\varphi}(\mathbf{r},\mathbf{r}'), \tag{21}$$

we obtain, instead of expression (19),

$$\begin{cases} -\nabla^2\tilde{\varphi} = 4\pi\delta^{(3)}(\mathbf{r}-\mathbf{r}'), & \text{outside spheroid,} \\ -\nabla^2\tilde{\varphi} = 0, & \text{inside spheroid.} \end{cases} \tag{22}$$

The continuity conditions for the tangential components of $\mathbf{E}$ and the normal components of $\mathbf{D}$ should be provided as well.

It is convenient to represent the solution of problem (22) in the form

$$\begin{cases} \tilde{\varphi} = \varphi_0 + \varphi_2, & \text{outside spheroid} \\ \tilde{\varphi} = \varphi_1, & \text{inside spheroid} \end{cases} \tag{23}$$

where φ_0 is the free-space potential given by

$$\varphi_0 = \frac{1}{|\mathbf{r}-\mathbf{r}'|}\,. \tag{24}$$

When solving electrostatic problem (22–24) for a prolate spheroid, it is quite natural to take its axis to be the z-axis of its coordinate system (see Fig. 2) [40]. The coordinate surfaces of this coordinate system ($\xi \geq 1 \geq \eta \geq -1$, $0 \leq \psi \leq 2\pi$) consist of oblong ellipsoids of revolution,

$$\frac{x^2+y^2}{f^2(\xi^2-1)} + \frac{z^2}{f^2\xi^2} = 1, \tag{25}$$

two-sheet hyperboloids of revolution,

$$\frac{x^2+y^2}{f^2(\eta^2-1)}+\frac{z^2}{f^2\eta^2}=1, \tag{26}$$

and planes,

$$y=x\tan\psi. \tag{27}$$

In equations (25, 26) and further, $2f$ is the distance between foci.

The ellipsoid of revolution with $\xi=\xi_0$ describes the nanospheroid under consideration.

The Cartesian coordinates are related to prolate spheroidal coordinates by the following relation:

$$\begin{aligned} x &= f\sqrt{(1-\eta^2)(\xi^2-1)}\cos\psi,\\ y &= f\sqrt{(1-\eta^2)(\xi^2-1)}\sin\psi,\\ z &= f\xi\eta. \end{aligned} \tag{28}$$

The metric coefficients for the prolate spheroidal coordinates are as follows:

$$\begin{aligned} g_\xi &= f\sqrt{\frac{(\xi^2-\eta^2)}{(\xi^2-1)}},\\ g_\eta &= f\sqrt{\frac{(\xi^2-\eta^2)}{(1-\eta^2)}},\\ g_\psi &= f\sqrt{(1-\eta^2)(\xi^2-1)}. \end{aligned} \tag{29}$$

The Green functions of free space (24) are given by [40]

$$\begin{aligned} \varphi_0 &= \frac{1}{|\mathbf{r}-\mathbf{r}'|}\\ &= \frac{1}{f}\sum_{n=0}^{\infty}\sum_{m=0}^{n}(2-\delta_{m0})(-1)^m(2n+1)\left[\frac{(n-m)!}{(n+m)!}\right]^2\\ &\quad\times P_n^m(\eta)P_n^m(\eta')\cos m(\psi-\psi')\\ &\quad\times\begin{cases} P_n^m(\xi)Q_n^m(\xi'), & \xi<\xi'\\ P_n^m(\xi')Q_n^m(\xi), & \xi>\xi' \end{cases}. \end{aligned} \tag{30}$$

In expression (30) and elsewhere, the letters P and Q stand for the associated Legendre functions of first and second kind [41]. Here the functions of η are defined on the interval $-1<\eta<1$, while those of $\xi>1$ have branch cut from minus infinity to 1.

It is convenient to represent (30) in the form

$$\begin{aligned} \varphi_0^{<} &= \frac{1}{f}\sum_{n=0}^{\infty}\sum_{m=0}^{n}P_n^m(\eta)P_n^m(\xi)\\ &\quad\times\left[\alpha_{nm}^{0,<}\cos m\psi+\beta_{nm}^{0,<}\sin m\psi\right], \quad \xi<\xi'\\ \varphi_0^{>} &= \frac{1}{f}\sum_{n=0}^{\infty}\sum_{m=0}^{n}P_n^m(\eta)Q_n^m(\xi)\\ &\quad\times\left[\alpha_{nm}^{0,>}\cos m\psi+\beta_{nm}^{0,>}\sin m\psi\right], \quad \xi>\xi' \end{aligned} \tag{31}$$

where the coefficients α^0 and β^0 are given by

$$\begin{aligned} \begin{Bmatrix}\alpha_{nm}^{0,<}\\ \beta_{nm}^{0,<}\end{Bmatrix} &= (2-\delta_{m0})(-1)^m(2n+1)\left[\frac{(n-m)!}{(n+m)!}\right]^2\\ &\quad\times P_n^m(\eta')Q_n^m(\xi')\begin{Bmatrix}\cos m\psi'\\ \sin m\psi'\end{Bmatrix}, \end{aligned} \tag{32}$$

$$\begin{aligned} \begin{Bmatrix}\alpha_{nm}^{0,>}\\ \beta_{nm}^{0,>}\end{Bmatrix} &= (2-\delta_{m0})(-1)^m(2n+1)\left[\frac{(n-m)!}{(n+m)!}\right]^2\\ &\quad\times P_n^m(\eta')P_n^m(\xi')\begin{Bmatrix}\cos m\psi'\\ \sin m\psi'\end{Bmatrix}. \end{aligned} \tag{33}$$

We will seek the solution of problem (22–24) in the region $\xi_0<\xi<\xi'$ (between the surface of the spheroid and the dipole) in the form

$$\begin{aligned} \tilde\varphi &= \frac{1}{f}\sum_{n=0}^{\infty}\sum_{m=0}^{n}P_n^m(\eta)P_n^m(\xi)\left[\alpha_{nm}^{0,<}\cos m\psi+\beta_{nm}^{0,<}\sin m\psi\right]\\ &\quad+\frac{1}{f}\sum_{n=0}^{\infty}\sum_{m=0}^{n}P_n^m(\eta)Q_n^m(\xi)\left[\alpha_{nm}^{(2)}\cos m\psi+\beta_{nm}^{(2)}\sin m\psi\right] \end{aligned} \tag{34}$$

and in the region $1<\xi<\xi_0$ (inside the spheroid) in the form

$$\begin{aligned} \tilde\varphi &= \frac{1}{f}\sum_{n=0}^{\infty}\sum_{m=0}^{n}P_n^m(\eta)P_n^m(\xi)\\ &\quad\times\left[\alpha_{nm}^{(1)}\cos m\psi+\beta_{nm}^{(1)}\sin m\psi\right] \end{aligned} \tag{35}$$

where $\alpha_{nm}^{(1)}$, $\beta_{nm}^{(1)}$, $\alpha_{nm}^{(2)}$, $\beta_{nm}^{(2)}$ are the coefficients to be found.

The continuity conditions for the tangential components of $\mathbf{E}$ and the normal components of $\mathbf{D}$ on the surface of the nanospheroid under consideration ($\xi=\xi_0$) yield the following system of equations

$$\begin{aligned} \alpha_{nm}^{(1)}P_n^m(\xi_0)-\alpha_{nm}^{(2)}Q_n^m(\xi_0) &= \alpha_{nm}^{0,<}P_n^m(\xi_0),\\ \varepsilon\alpha_{nm}^{(1)}\frac{\mathrm{d}}{\mathrm{d}\xi_0}P_n^m(\xi_0)-\alpha_{nm}^{(2)}\frac{\mathrm{d}}{\mathrm{d}\xi_0}Q_n^m(\xi_0) &= \alpha_{nm}^{0,<}\frac{\mathrm{d}}{\mathrm{d}\xi_0}P_n^m(\xi_0). \end{aligned} \tag{36}$$

A similar system is also valid for the coefficients β.

The solution of system (36) is

$$\begin{aligned} \alpha_{nm}^{(2)} &= \frac{(\varepsilon-1)P_n^m(\xi_0)\frac{\mathrm{d}}{\mathrm{d}\xi_0}P_n^m(\xi_0)}{P_n^m(\xi_0)\frac{\mathrm{d}}{\mathrm{d}\xi_0}Q_n^m(\xi_0)-\varepsilon Q_n^m(\xi_0)\frac{\mathrm{d}}{\mathrm{d}\xi_0}P_n^m(\xi_0)}\alpha_{nm}^{0,<}\\ &= G_{nm}\alpha_{nm}^{0,<},\\ \beta_{nm}^{(2)} &= G_{nm}\beta_{nm}^{0,<}. \end{aligned} \tag{37}$$

It is important to note that expressions (37) do not exist for some real negative values of permittivity, and so the

solution of the quasistatic problem is also nonexistent [42]. In that case, as well as in the case of dielectric sphere [42], there appears a polariton (or plasmon) resonance. This situation can be described within the framework of a fully electrodynamic approach. Nevertheless, it is obvious that such conditions result in a substantial increase of the decay rates, as in the case with the sphere [27]. We will analyse this effect in the next section.

In the case of ideally conducting spheroid (*i.e.*, one with $\varepsilon \to \infty$), one should use in (37) the following expression instead of G_{nm}:

$$G_{nm}^{\text{ideal}} = -\frac{P_n^m(\xi_0)}{Q_n^m(\xi_0)}\,. \tag{38}$$

Now, taking into account expressions (31, 34), we can write the dipole potential in the region $\xi > \xi'$ in the form

$$\tilde{\varphi} = \frac{1}{f}\sum_{n=0}^{\infty}\sum_{m=0}^{n} P_n^m(\eta)Q_n^m(\xi)\left[(\alpha_{nm}^{0,>} + G_{nm}\alpha_{nm}^{0,<})\cos m\psi \right. \\ \left. +(\beta_{nm}^{0,>} + G_{nm}\beta_{nm}^{0,<})\sin m\psi\right]. \tag{39}$$

Using expressions (12, 13), one can find from (39) both the reflected field, to determine the frequency shift of interest, and the total dipole momentum, to find the decay rate.

3.2 General expression for radiative decay rates

To determine the total dipole momentum, one should find the asymptote of (39) in the far field, that is, for $\xi \to \infty$. One can see that the main contribution is due to the terms with $n = 0$ and $n = 1$ (dipole radiation). Using the fact that in the far field $\xi \approx R/f$, $\eta \approx \cos\theta$, (R, θ, ψ are spherical coordinates), and that the asymptotes of Legendre functions are

$$Q_1(\xi) = \frac{\xi}{2}\ln\frac{\xi+1}{\xi-1} - 1 \cong \frac{1}{3\xi^2} \\ Q_1^1(\xi) = \sqrt{\xi^2-1}\frac{\mathrm{d}Q_1(\xi)}{\mathrm{d}\xi} \cong -\frac{2}{3\xi^2} \tag{40}$$

we obtain the following asymptote ($\xi \to \infty$) for the potential of a unit charge (39) in the presence of a prolate spheroid:

$$\tilde{\varphi} \cong \frac{1}{R} + \frac{f}{R^2}\left[\begin{array}{l} P_1(\eta')P_1(\xi')\left(1 + G_{10}\dfrac{Q_1(\xi')}{P_1(\xi')}\right)\cos\theta \\ +P_1^1(\eta')P_1^1(\xi')\left(1 + G_{11}\dfrac{Q_1^1(\xi')}{P_1^1(\xi')}\right) \\ \qquad \times \sin\theta\cos(\psi - \psi') \end{array}\right]. \tag{41}$$

Accordingly, for the dipole potential, we have

$$\varphi = (\mathbf{d}_0\nabla')\tilde{\varphi}. \tag{42}$$

Comparing the differentiation result with the well-known dipole potential

$$\varphi_{\text{dip}} = \frac{(\mathbf{d}_{\text{tot}}\mathbf{R})}{R^3}, \tag{43}$$

one can find the total dipole momentum of the oscillator + spheroid system. Without any loss of generality, we assume that the dipole is placed at $\psi' = 0$ (cylindrical symmetry).

For the ξ-orientation of the dipole, that is for the orientation which is normal to the ellipsoid defined by equation (25) with $\xi = const$ (see Fig. 1), the potential at large separations is given by ($\psi' = 0$)

$$\varphi^{>} \cong \frac{d_{0,\xi'}}{g_{\xi'}}\frac{\partial}{\partial\xi'}\tilde{\varphi}^{>} = \frac{d_{0,\xi'}}{R^2}\sqrt{\frac{(\xi'^2-1)}{(\xi'^2-\eta'^2)}} \\ \times\left[\begin{array}{l} \eta'\left(1 + G_{10}\dfrac{\mathrm{d}}{\mathrm{d}\xi'}(Q_1(\xi'))\right)\cos\theta \\ +\sqrt{1+\eta'^2}\left(\dfrac{\xi'}{\sqrt{\xi'^2-1}} + G_{11}\dfrac{\mathrm{d}}{\mathrm{d}\xi'}(Q_1^1(\xi'))\right) \\ \qquad \times \sin\theta\cos\psi \end{array}\right]. \tag{44}$$

One can find from (44) the Cartesian components of the total dipole momentum:

$$d_{\text{tot},z} = d_{0,\xi'}\sqrt{\frac{(\xi'^2-1)}{(\xi'^2-\eta'^2)}}\eta'\left(1 + G_{10}\frac{\mathrm{d}}{\mathrm{d}\xi'}Q_1(\xi')\right), \\ d_{\text{tot},x} = d_{0,\xi'}\sqrt{\frac{(\xi'^2-1)}{(\xi'^2-\eta'^2)}})\sqrt{1-\eta'^2} \\ \times\left(\frac{\xi'}{\sqrt{\xi'^2-1}} + G_{11}\frac{\mathrm{d}}{\mathrm{d}\xi'}Q_1^1(\xi')\right). \tag{45}$$

Taking into account the fact that the first terms in (45) are due to the free oscillator, we find with the help of (18) the radiative decay rate for the ξ-orientation of the dipole momentum of the oscillator ($d_{0,z}^2 + d_{0,x}^2 = d_{0,\xi'}^2$):

$$\left(\frac{\gamma}{\gamma_0}\right)_{\xi} = \frac{|d_{\text{tot},z}|^2 + |d_{\text{tot},x}|^2}{d_{0,z}^2 + d_{0,x}^2} \\ = \frac{(\xi'^2-1)}{(\xi'^2-\eta'^2)}\left[\eta'^2\left(1 + G_{10}\frac{\mathrm{d}}{\mathrm{d}\xi'}Q_1(\xi')\right)^2 \right. \\ \left. +(1-\eta'^2)\left(\frac{\xi'}{\sqrt{\xi'^2-1}} + G_{11}\frac{\mathrm{d}}{\mathrm{d}\xi'}Q_1^1(\xi')\right)^2\right]. \tag{46}$$

The decay rates for the η- and ψ-orientations of the dipole momentum, that is for the orientations which are normal to hyperboloids (Eq. (26)) and planes (Eq. (27)) (see also

Fig. 1), can be obtained in the same way:

$$\left(\frac{\gamma}{\gamma_0}\right)_\eta = \frac{\eta'^2(\xi'^2-1)\left|1+G_{11}\dfrac{Q_1^1(\xi')}{\sqrt{\xi'^2-1}}\right|^2}{(\xi'^2-\eta'^2)} + \frac{(1-\eta'^2)\xi'^2\left|1+G_{10}\dfrac{Q_1(\xi')}{\xi'}\right|^2}{(\xi'^2-\eta'^2)}, \quad (47)$$

$$\left(\frac{\gamma}{\gamma_0}\right)_\psi = \left|1+G_{11}\frac{Q_1^1(\xi')}{\sqrt{\xi'^2-1}}\right|^2 . \quad (48)$$

The coefficients G_{10} and G_{11} are defined by expression (37), and for specific indices, they take on the following form:

$$G_{10} = \frac{(\varepsilon-1)\xi_0}{\xi_0\dfrac{\mathrm{d}}{\mathrm{d}\xi_0}Q_1(\xi_0) - \varepsilon Q_1(\xi_0)}, \quad (49)$$

$$G_{11} = \frac{(\varepsilon-1)\xi_0}{\sqrt{\xi_0^2-1}\dfrac{\mathrm{d}}{\mathrm{d}\xi_0}Q_1^1(\xi_0) - \varepsilon\xi_0\dfrac{\mathrm{d}}{\mathrm{d}\xi_0}Q_1(\xi_0)} . \quad (50)$$

It is worthy to note that expressions (46–48) describe only *radiative* decay rates which are not equal to the total decay rate in the case of spheroid with internal losses (with a complex permittivity).

In the case of ideally conducting spheroid, we have the following expressions instead of (49, 50):

$$G_{10} = -\frac{\xi_0}{Q_1(\xi_0)}; \quad G_{11} = -\frac{1}{\mathrm{d}Q_1(\xi_0)/\mathrm{d}\xi_0} . \quad (51)$$

The results are substantially simplified when the distance between an atom and a spheroid is much larger than the spheroid size but still remains much less than the wavelength, *i.e.* one can limit the multipole expansion of the field of the atomic dipole to the first term. It corresponds to the $\xi' \to \infty$ regime in the preceding formulae. By substituting the expansion of (41) over $1/\xi'$ into (42), it is possible to find with the help of (43) the expression for the total dipole momentum of the system

$$d_{\mathrm{tot},i} = d_{0,i} + P_{ij}^{\mathrm{sph}} M_{jk} d_{0,k} \quad (52)$$

where the indices $i,j,k = 1...3$ correspond to Cartesian co-ordinates and P^{sph} and M tensors have the following form

$$P_{ij}^{\mathrm{sph}} = \frac{f^3}{3}\begin{bmatrix} 2G_{11} & 0 & 0 \\ 0 & 2G_{11} & 0 \\ 0 & 0 & -G_{10} \end{bmatrix}_{i,j}$$

$$M_{ij} = -\frac{\delta_{ij}}{r'^3} + 3\frac{r'_i r'_j}{r'^5} .$$

Naturally, the expression (52) coincides with the expression for the total dipole momentum of the system, consisting of the atomic dipole and the point-like, induced dipole of the nanospheroid, with P^{sph} as polarizability tensor. Note, that $M_{jk}d_{0,k}$ is the electric field of the atomic dipole at the nanospheroid position. This coincidence confirms the correctness of our calculations. Substituting (52) into (18) it is possible to find the decay rates for arbitrary relative orientation of the atom dipole momentum and the spheroid axis.

3.3 General expression for frequency shifts

Let us now consider the frequency shift. According to expression (17), the frequency shift is governed by the reflected field $\mathbf{d}_0\mathbf{E}^{(\mathrm{R})}(\mathbf{r},\omega_0)$ that can be found from expressions (21, 39):

$$\mathbf{d}_0\mathbf{E}^{(\mathrm{R})}(\mathbf{r},\omega) = -(\mathbf{d}_0\nabla)(\mathbf{d}_0\nabla')\tilde{\varphi}^{\mathrm{R}}(\mathbf{r},\mathbf{r}') \quad (53)$$

$$\tilde{\varphi}^{\mathrm{R}}(\mathbf{r},\mathbf{r}') = \sum_{n=0}^{\infty}\sum_{m=0}^{n} P_n^m(\eta)Q_n^m(\xi)G_{nm}[\alpha_{nm}^{0,<}(\mathbf{r}')\cos m\psi + \beta_{nm}^{0,<}(\mathbf{r}')\sin m\psi], \quad \xi > \xi'. \quad (54)$$

Expression (53) describes the term a_1 in expansion (11).

Let us now consider the ξ-orientation of the dipole momentum of the oscillator. From expressions (53, 54) we get

$$\mathbf{d}_0\mathbf{E}^{(\mathrm{R})}(\mathbf{r}',\omega_0) = -\frac{d_\xi d_{\xi'}}{g_\xi g_{\xi'}}\sum_{n=0}^{\infty}\sum_{m=0}^{n} P_n^m(\eta)\frac{\mathrm{d}}{\mathrm{d}\xi}Q_n^m(\xi)G_{nm}\left[\frac{\mathrm{d}}{\mathrm{d}\xi'}\alpha_{nm}^{0,<}(\mathbf{r}')\right]. \quad (55)$$

Now, putting $\xi = \xi'$, $\eta = \eta'$, $\psi = \psi' = 0$ in expression (55) to find the reflected field at the dipole position and using equation (9), we obtain the final expression for the frequency shift of an oscillator with the ξ-orientation of its dipole momentum:

$$\left(\frac{\Delta\omega}{\gamma_0}\right)_\xi = \frac{3}{4(k_0f)^3}\frac{(\xi'^2-1)}{(\xi'^2-\eta'^2)}\sum_{n=1}^{\infty}\sum_{m=0}^{n}(2-\delta_{m0})(-1)^m(2n+1) \times \mathrm{Re}(G_{nm})\left(\frac{(n-m)!}{(n+m)!}P_n^m(\eta')\frac{\mathrm{d}}{\mathrm{d}\xi}Q_n^m(\xi')\right)^2 . \quad (56)$$

Expressions for the frequency shifts in the case of η- and ψ-orientations can be obtained in the same way:

$$\left(\frac{\Delta\omega}{\gamma_0}\right)_\eta = \frac{3}{4d_\eta^2k_0^3}\frac{d_\eta d_{\eta'}}{g_\eta g_{\eta'}}\frac{\mathrm{d}^2}{\mathrm{d}\eta\mathrm{d}\eta'}\tilde{\varphi}^{>,\mathrm{R}}(\mathbf{r},\mathbf{r}')\Big|_{\mathbf{r}=\mathbf{r}'} = \frac{3}{4(k_0f)^3}\frac{(1-\eta'^2)}{(\xi'^2-\eta'^2)}\sum_{n=1}^{\infty}\sum_{m=0}^{n}(2-\delta_{m0})(-1)^m(2n+1) \times \mathrm{Re}(G_{nm})\left(\frac{(n-m)!}{(n+m)!}Q_n^m(\xi)\frac{\mathrm{d}}{\mathrm{d}\eta}P_n^m(\eta)\right)^2 , \quad (57)$$

$$\left(\frac{\Delta\omega}{\gamma_0}\right)_{\psi} = \frac{3}{4d_\psi^2 k_0^3}\frac{d_\psi d_{\psi'}}{g_\psi g_{\psi'}}\frac{\mathrm{d}^2}{\mathrm{d}\psi\mathrm{d}\psi'}\tilde{\varphi}^{>,\mathrm{R}}(\mathbf{r},\mathbf{r}')\Big|_{\mathbf{r}=\mathbf{r}'} = \frac{3}{4(k_0 f)^3}\frac{1}{(1-\eta'^2)(\xi'^2-1)}\sum_{n=1}^{\infty}\sum_{m=0}^{n}(2-\delta_{m0})(-1)^m(2n+1) \times G_{nm}\left(m\frac{(n-m)!}{(n+m)!}Q_n^m(\xi)P_n^m(\eta)\right)^2. \quad (58)$$

Expressions (46–48) for the radiative decay rates and (56–58) for the frequency shifts occurring in the presence of a prolate nanospheroid are the main result of this paper and can be applied to a number of situations of practical interest.

As already mentioned in the preceding section, expressions (46–48) and (56–58) are the leading terms of the expansions of the near and the far field in the quasistatic approximation. One should take this fact into account in the case of spheroid with internal losses, where the near fields contribute to the total decay rate. Substituting expression (38) into (56–58), one arrives at the case of ideally conducting spheroid

4 Decay rates in particular cases

The results obtained in the preceding section are rather general and complicated. It is worth considering some particular cases. The following cases are of interest from the physical point of view:

(a) an atom on the axis of a spheroid ($\eta = 1$) (see Fig. 1a, needle tip model);
(b) an atom near the equator of a spheroid ($\eta = 0$) (see Fig. 1b);
(c) a sphere limit ($\xi_0 = \infty$);
(d) a needle limit ($\xi_0 = 1$);
(e) an ideally conducting spheroid.

Throughout this section, all primes on the oscillator location coordinates will be dropped with no misunderstanding being caused.

4.1 Radiative decay of an atom

General expressions (46–48) are greatly simplified in the case of atom on the axis of a spheroid ($\eta = 1$):

$$\left(\frac{\gamma}{\gamma_0}\right)_{\xi,\eta=1} = \left|1 + G_{10}\frac{\mathrm{d}}{\mathrm{d}\xi}Q_1(\xi)\right|^2, \quad (59)$$

$$\left(\frac{\gamma}{\gamma_0}\right)_{\eta,\eta=1} = \left(\frac{\gamma}{\gamma_0}\right)_{\psi,\eta=1} = \left|1 + G_{11}\frac{\mathrm{d}}{\mathrm{d}\xi}Q_1(\xi)\right|^2. \quad (60)$$

Accordingly, in the case of atom near the equator of a spheroid ($\eta = 0$), we have

$$\left(\frac{\gamma}{\gamma_0}\right)_{\xi,\eta=0} = \left|1 + G_{11}\frac{\sqrt{\xi^2-1}}{\xi}\frac{\mathrm{d}}{\mathrm{d}\xi}Q_1^1(\xi)\right|^2, \quad (61)$$

$$\left(\frac{\gamma}{\gamma_0}\right)_{\eta,\eta=0} = \left|1 + G_{10}\frac{Q_1(\xi)}{\xi}\right|^2, \quad (62)$$

$$\left(\frac{\gamma}{\gamma_0}\right)_{\psi,\eta=0} = \left|1 + G_{11}\frac{\mathrm{d}}{\mathrm{d}\xi}Q_1(\xi)\right|^2. \quad (63)$$

The most interesting feature of the decay rate of a ψ-oriented dipole is its independence of the η-coordinate.

Further simplification can be achieved if one considers the case where the atom is located in close vicinity of the spheroid surface ($\xi \to \xi_0$). In that case, one can get, instead of (59–63), the following expressions for an atom located near the tip of a prolate spheroid ($\eta = 1$):

$$\left(\frac{\gamma}{\gamma_0}\right)_{\xi,\eta=1} = \left|\frac{2\varepsilon}{\left(\xi_0(\varepsilon-1)(\xi_0^2-1)\ln\frac{\xi_0+1}{\xi_0-1} + 2(\varepsilon+\xi_0^2-\xi_0^2\varepsilon)\right)}\right|^2 \quad (64)$$

$$\left(\frac{\gamma}{\gamma_0}\right)_{\eta,\eta=1} = \left(\frac{\gamma}{\gamma_0}\right)_{\psi,\eta=1} = \left|\frac{4}{\left(\xi_0(\varepsilon-1)(\xi_0^2-1)\ln\frac{\xi_0+1}{\xi_0-1} + 2(\xi_0^2-\xi_0^2\varepsilon-2)\right)}\right|^2 \quad (65)$$

and for an atom near the spheroid equator ($\eta = 0$):

$$\left(\frac{\gamma}{\gamma_0}\right)_{\xi,\eta=0} = \left|\frac{4\varepsilon}{\left(\xi_0(\varepsilon-1)(\xi_0^2-1)\ln\frac{\xi_0+1}{\xi_0-1} + 2(\xi_0^2-\xi_0^2\varepsilon-2)\right)}\right|^2 \quad (66)$$

$$\left(\frac{\gamma}{\gamma_0}\right)_{\eta,\eta=0} = \left|\frac{2}{\left(\xi_0(\varepsilon-1)(\xi_0^2-1)\ln\frac{\xi_0+1}{\xi_0-1} + 2(\varepsilon+\xi_0^2-\xi_0^2\varepsilon)\right)}\right|^2 \quad (67)$$

$$\left(\frac{\gamma}{\gamma_0}\right)_{\psi,\eta=0} = \left|\frac{4}{\left(\xi_0(\varepsilon-1)(\xi_0^2-1)\ln\frac{\xi_0+1}{\xi_0-1} + 2(\xi_0^2-\xi_0^2\varepsilon-2)\right)}\right|^2. \quad (68)$$

Analyzing these expressions, one can find the following regularity that holds true for spheroids of any shape: the ξ-decay rate near the pole, (64), exceeds the η-decay rate

Table 1. Relative radiative decay rates of an atomic oscillator placed on the surface of a spheroid $\xi \to \xi_0$ for various dipole positions and orientations and for limiting spheroid shapes.

		vertex ($\eta = 1$)		equator ($\eta = 0$)	
orientation	spheroid shape	dielectric	ideal conductor	dielectric	ideal conductor
ξ	sphere	$\left\lvert\frac{3\varepsilon}{2+\varepsilon}\right\rvert^2$	9	$\left\lvert\frac{3\varepsilon}{2+\varepsilon}\right\rvert^2$	9
	needle	$\lvert\varepsilon\rvert^2$	$\left(\left(\ln\frac{2}{\xi_0-1}-2\right)(\xi_0-1)\right)^{-2}$ $\xi_0\to 1$	$\left\lvert\frac{2\varepsilon}{1+\varepsilon}\right\rvert^2$	4
η	sphere	$\left\lvert\frac{3}{2+\varepsilon}\right\rvert^2$	0	$\left\lvert\frac{3}{2+\varepsilon}\right\rvert^2$	0
	needle	$\left\lvert\frac{2}{1+\varepsilon}\right\rvert^2$	0	1	0
ψ	sphere	$\left\lvert\frac{3}{2+\varepsilon}\right\rvert^2$	0	$\left\lvert\frac{3}{2+\varepsilon}\right\rvert^2$	0
	needle	$\left\lvert\frac{2}{1+\varepsilon}\right\rvert^2$	0	$\left\lvert\frac{2}{1+\varepsilon}\right\rvert^2$	0

near the equator, (67), by a factor of ε^2. Similarly, decay rate (66) exceeds that defined by expressions (65, 68) by a factor of ε^2, too.

The above formulas (64–68) are valid for prolate spheroids of any shape, *i.e.*, for any ξ_0. However, it is of interest to study the linewidth behaviour in the particular cases of sphere ($\xi_0 \to \infty$) and needle ($\xi_0 \to 1$). For the sake of clarity, it is convenient to tabulate various asymptotes (see Tab. 1).

The analysis of this table shows that the decay rates for the spherical limit case coincide with those obtained from the exact solution for a dielectric sphere [15]. Of more interest is comparison with the results obtained when investigating a dipole radiation near an infinite circular cylinder [23]. In the case of dielectric cylinder whose radius is small in comparison with the radiation wavelength, the decay rates coincide with those for an atom placed near the equator of a highly prolate spheroid. Such a coincidence is an additional confirmation of the correctness of our calculations.

As to an ideally conducting cylinder, the result for a radially-oriented dipole differs from that in the case of spheroid (ξ-orientation). According to [23], the decay rate for an ideally conducting cylinder of small radius tends to infinity:

$$\left(\frac{\gamma}{\gamma_0}\right)_{\mathrm{dip},\rho} \xrightarrow[kb=ka\to 0]{} \frac{3}{2(ka)^2}\left[1+\frac{2}{\pi}\arctan(L^*) + \frac{4(\ln 2-1)}{\pi^2(1+L^{*2})}+\ldots\right]+4+\ldots$$

$$L^* = \frac{2}{\pi}\left(\ln\left(\frac{ka}{2}\right)+0.5772\right) \qquad (69)$$

while in the case of ideally conducting needle ($\xi_0 \to 1$), the decay rate is finite:

$$\left(\frac{\gamma}{\gamma_0}\right)_{\xi} \longrightarrow 4... \qquad (70)$$

This difference is due to the fact that, in the case of ideally conducting cylinder, a current wave is excited in a spatial domain whose characteristic size is much greater than the radiation wavelength [23]. In that case, the quasistatic approximation is not valid, and so one cannot compare between the dipole radiation of an oscillator placed near a small spheroid and that of an oscillator near an infinite cylinder.

The radiation of a ξ-oriented dipole located at the tip ($\eta = 1$) of a prolate spheroid is of particular interest. As it can be seen from Table 1, as the permittivity gets larger, the relative decay rate increases in a square-law fashion. In the case of ideally conducting spheroid, one can see from the table that the decay rate increases unboundedly as the spheroid tapers off into an infinitely thin needle ($\xi = \xi_0 \to 1, \eta = 1$). This fact has a simple physical explanation: any field in the vicinity of a sharp metal tip is infinitely enhanced. A similar unbounded increase of the decay rate also obtains in the case of dipole near a conical needle tip [24].

Another interesting feature seen in Table 1 is the fact that when the dipole is located at the equator of the spheroid and oriented along its axis, the ideally conducting case fails to agree with the limit $\varepsilon = \infty$.

In the remaining cases, one can change over from the dielectric to the ideally conducting case by simply equating the permittivity to infinity. Note that in the case of ideally conducting spheroid the decay rates for the tangential dipole orientations (ψ- and η-orientations) are always equal to zero.

The relationships between the relative linewidth γ/γ_0 and the distance $(\xi - \xi_0)$ of the atom from the surface of dielectric nanospheroid with $\varepsilon = 3$, $\xi_0 = 1.1$ and $\xi_0 = 3$, for various dipole orientations and atom positions with respect to the spheroid surface are presented in Figures 3 and 4. One can see from these figures that the decay rates for the highly prolate spheroid (Fig. 3) depend strongly on the dipole orientation.

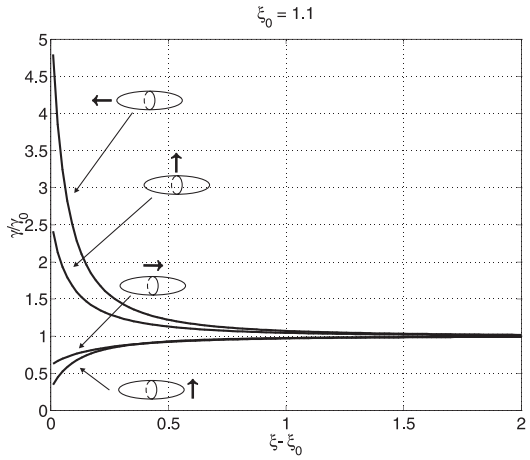

Fig. 3. Relative linewidth γ/γ_0 as a function of the distance of the dipole from the surface of the spheroid for various dipole orientations and atomic positions (ξ) in the case of dielectric spheroid with $\varepsilon = 3$ and $\xi_0 = 1.1$. Arrows indicate the position and orientation of the dipole.

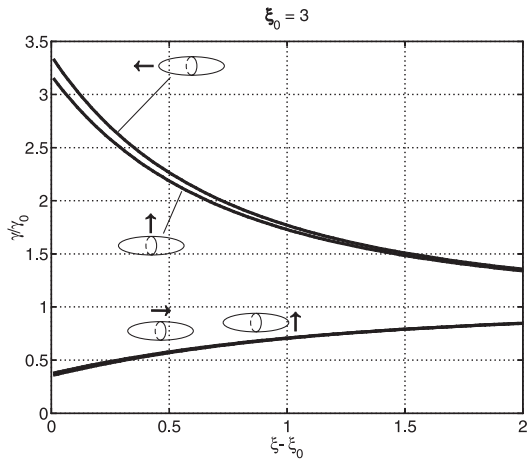

Fig. 4. Relative linewidth γ/γ_0 as a function of the distance of the dipole from the surface of the spheroid for various dipole orientations and atomic positions (ξ) in the case of dielectric spheroid with $\varepsilon = 3$ and $\xi_0 = 3$. Arrows indicate the position and orientation of the dipole.

As the spheroid eccentricity decreases (Fig. 4), the decay rates for the ξ- and η-oriented dipoles become less dependent on the η-coordinate. Another important feature is that the decay rate for the ξ-oriented dipole always exceeds that for the η-oriented dipole.

It is clear from Figures 3 and 4 that the radiative decay rate can be both increased ($\gamma > \gamma_0$) and reduced ($\gamma < \gamma_0$). The decay enhancement effect is obtained when the dipole orientation is perpendicular to spheroid surface, and is more important with the dipole located near the acute end of the spheroid. The decay suppression effect occurs when the dipole orientation is parallel to spheroid surface, and is again most pronounced with the dipole near the acute end of the spheroid. These effects are clear manifestations of the influence of surface curvature on the radiative decay of an atom in the vicinity of the surface of a spheroid. Note that decay enhancement and suppression can be simply interpreted *via* by the dipole image induced in the nanobody, which is either parallel or antiparallel to the atomic dipole.

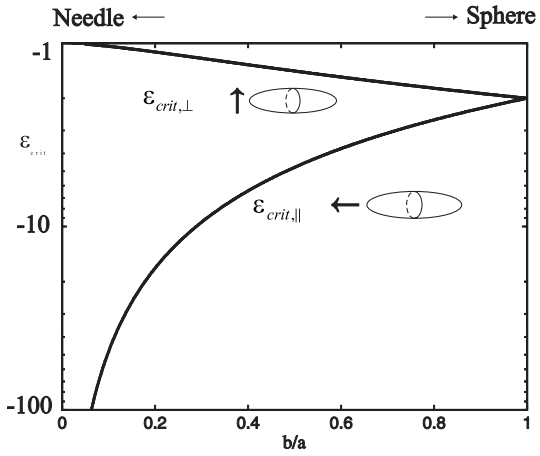

Fig. 5. Relationships (71, 72) between the critical permittivity allowing a polariton or plasmon resonance to occur and the ratio b/a between the axes of the spheroid.

4.2 Radiative and radiationless decay rates for a metal nanospheroid

As in the case of a microsphere, there are critical values of the spheroid permittivity for which the static problem (Eqs. (22–24)) has no solution and the field inside the spheroid undergoes a significant increase. This case is usually referred to as a polariton or plasmon resonance [42,43]. However, in contrast to the spherical case, the critical permittivity values here depend both on the dipole orientation and the shape of the spheroid.

Generally speaking, there are two critical values of permittivity for which the plasmon resonance occur. The first critical value is determined such that G_{10} becomes infinite (see Eq. (49)):

$$\varepsilon_{\mathrm{crit},\parallel} = \xi_0 \frac{\dfrac{\mathrm{d}}{\mathrm{d}\xi_0} Q_1(\xi_0)}{Q_1(\xi_0)} \tag{71}$$

while the second one is determined such that G_{11} becomes infinite (see Eq. (50)):

$$\varepsilon_{\mathrm{crit},\perp} = (\xi_0^2 - 1) \frac{\dfrac{\mathrm{d}}{\mathrm{d}\xi_0} Q_1^1(\xi_0)}{\xi_0 Q_1^1(\xi_0)} \cdot \tag{72}$$

The relations (71, 72), as functions of the the ratio $b/a = \sqrt{(\xi_0^2 - 1)}/\xi_0$ between the spheroid axes, are shown in Figure 5. One can see from this figure that $\varepsilon_{\mathrm{crit},\parallel}$ and $\varepsilon_{\mathrm{crit},\perp}$ vary from $-\infty$ to -2 and from -1 to -2 respectively, as the nanospheroid is transformed from needle-like to spherical shape.

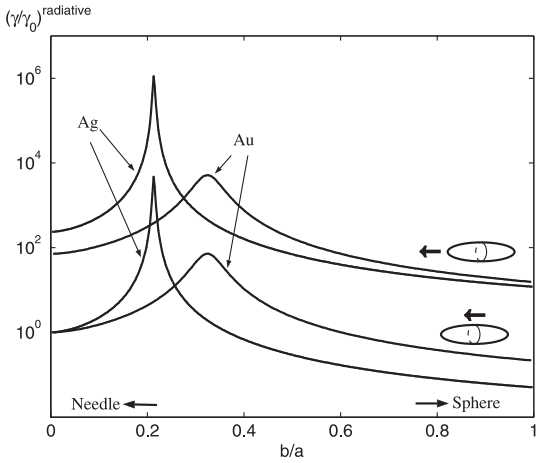

Fig. 6. Relative decay rates (in logarithmic scale) as a function of the ratio b/a between the axes of spheroids made of gold (Au: $\varepsilon = -8.37 + \mathrm{i}1.16$, $\lambda = 600$ nm [44]) and silver (Ag: $\varepsilon = -15.37 + \mathrm{i}0.231$ [45], $\lambda = 632.8$ nm). The dipole is parallel to the major axis of the spheroid.

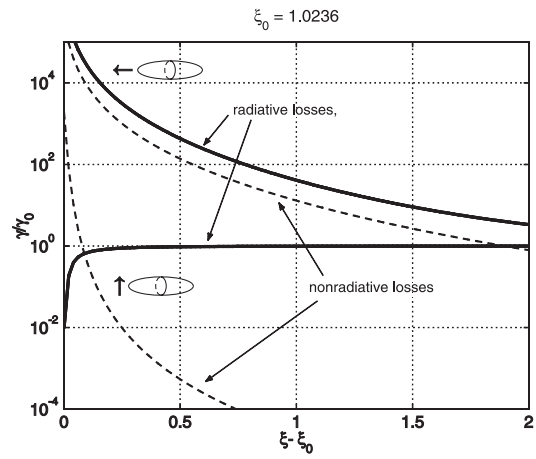

Fig. 7. Relative radiative and radiationless decay rates as a function of the distance between a ξ- or η-oriented dipole and the surface of a silver spheroid (Ag: $\varepsilon = -15.37 + \mathrm{i}0.231$, $\lambda = 632.8$ nm) in the case of plasmon resonance ($\xi_0 = 1.0236$). The dipole is located at the vertex of the spheroid ($\eta = 1$), and we take half the distance between the spheroid foci to be $f = 0.1\lambda$.

It is interesting to note, that the situation is simplified for two particular atom positions (on the axis and on the equator). In this case there is only one critical value of permittivity, (71) or (72), when the dipole is oriented along the major axis of the spheroid or perpendicularly to it.

In Figure 6, the radiative decay rates of an oscillator oriented along the major axis of a spheroid made of silver (Ag: $\varepsilon = -15.37 + \mathrm{i}0.231$, $\lambda = 632.8$ nm [44]) or gold (Au: $\varepsilon = -8.37 + \mathrm{i}1.16$, $\lambda = 600$ nm [45]) are shown as a function of the ratio b/a. It is evident from the figure that there takes place a dramatic enhancement of the decay rates for the silver spheroid with $b/a = 0.213$ ($\xi_0 = 1.0236$) and for the gold spheroid with $b/a = 0.325$ ($\xi_0 = 1.057$). This enhancement agrees qualitatively with the experimental results obtained in [28], where fluorescence was found to increase substantially in the presence of golden nanorods.

It should be noted that the above substantial enhancement of the radiative decay rates should be regarded as the first estimation only. Firstly, the quasistatic approximation we used may not be applicable here. Indeed, the quasistatic approximation is valid only if $ka \ll 1$ and permittivity ε is far from critical value, $(ka)^2 \ll |\varepsilon - \varepsilon_{\mathrm{crit}}|$. Fortunately, in our case, the minimal value of $|\varepsilon - \varepsilon_{\mathrm{crit}}|$ is equal to imaginary part of permittivity ε'', $|\varepsilon - \varepsilon_{\mathrm{crit}}| \approx |\varepsilon''|$. As a result the quasistatic approximation will be valid even in the case of silver, because the additional condition $(ka)^2 \ll |\varepsilon''| \approx 0.23$ can be easily fulfilled. Secondly, even when the quasistatic approximation is valid, this substantial enhancement (by factor 10^6 for Ag) is questionable, because the main perturbative formula (8) is valid if the decay rates are small in comparison with the radiation frequency and other characteristic frequencies (resonance width etc.). For E1-allowed transition the enhancement by factor 10^6 gives a decay rate comparable with the radiation frequency and one should consider higher orders of perturbation theory.

Up to now we have considered *radiative* decay rates. To estimate *radiationless* decay rates, one should use general expression (16). For a ξ-oriented dipole located on the axis of a spheroid, the radiative decay rates can be found with the help of expressions (16, 56, 59):

$$\begin{aligned}\left(\frac{\gamma}{\gamma_0}\right)^{\mathrm{losses}}_{\xi,\eta=1} &= \left(\frac{\gamma}{\gamma_0}\right)^{\mathrm{total}}_{\xi,\eta=1} - \left(\frac{\gamma}{\gamma_0}\right)^{\mathrm{radiative}}_{\xi,\eta=1} \\ &= \frac{3}{2}\mathrm{Im}\left(\frac{a_1}{k_0^3}\right) + \mathrm{Re}\left(1+\frac{3}{2}d_1\right) - \left|1+\frac{3}{2}d_1\right| \\ &= -2\left(\mathrm{Im}(G_{10})\frac{\mathrm{d}}{\mathrm{d}\xi}Q_1(\xi)\right)^2 - \frac{3}{2(k_0 f)^3}\sum_{n=1}^{\infty}(2n+1) \\ &\quad \times\left\{\mathrm{Im}(G_{n0})\left(\frac{\mathrm{d}}{\mathrm{d}\xi}Q_n(\xi)\right)^2 + O((kf)^2)\right\}. \qquad (73)\end{aligned}$$

In the limit ξ, $\xi_0 \to \infty$, this expression agrees with the one found for spherical particles [15,27]. In the case of real permittivity, the losses occurring inside a nanospheroid go to zero, as it must be. However, in the case of nanobodies of complex permittivity internal loss (73) can become predominant in comparison with radiative loss (59). The dependence of the radiative and non-radiatiative decay rates of a dipole located on the axis of a spheroid on the distance between the dipole and the spheroid surface is shown in Figure 7. Here we consider the case of plasmon resonance ($\xi_0 = 1.0236$) for a silver spheroid (Ag: $\varepsilon = -15.37 + \mathrm{i}0.231$, $\lambda = 632.8$ nm [44]) with the major semiaxis $a \approx f = 0.1\lambda$. The minor semiaxis of the spheroid is $b \approx 0.02\lambda$. Note that a plasmon resonance in this case occurs mainly with a dipole whose dipole momentum is oriented parallel to the major spheroid axis.

One can see from Figure 7 that in the case of ξ-oriented dipole the radiative loss exceeds the radiationless one for all distances $\xi - \xi_0 > 0.01$. The situation with an η-oriented dipole is different. In the region $\xi - \xi_0 < 0.1$,

the non-radiative processes dominate because of the predominance of the near-field coupling between the atomic dipole and polaritons.

In general, the case of an atom near a spheroid occupies an intermediate position between the spherical and the cylindrical case. This allows us to use a nanospheroid as an effective tool to control the radiative and radiationless decay rates of an excited atom.

An important feature of nanospheroids is the possibility of tuning their plasmon resonances for various media by changing their shape, *i.e.*, by changing their b/a ratio. On the one hand, this allows one to control spontaneous decay processes and, on the other, makes it possible to measure the complex permittivity of their material.

4.3 Prolate nanospheroid as a model of a needle tip in an apertureless scanning optical microscope [46]

A prolate nanospheroid can be treated as a model of a needle tip used in a apertureless scanning microscope. On the other hand, an excited atomic oscillator near the spheroid can be considered as an object. In this model radiation power can be regarded as the scanning signal. That is why it is interesting to know the relationship between radiative losses and the displacement of the atom relative to the spheroid. For the sake of definiteness, we suppose that the atomic dipole is oriented vertically (along the z-axis) and is moved along the x-axis. In doing so, the minimal distance h between the atom and the pole of the spheroid can be varied. The geometry of such a scanning microscope is shown in Figure 8.

In this case, the spheroidal coordinates of the atom are the following functions of Δx and h:

$$\xi^2 = \frac{(\xi_0 + h/f)^2 + (\Delta x/f)^2 + 1}{2} + \frac{\sqrt{((\xi_0 + h/f)^2 + (\Delta x/f)^2 + 1)^2 - 4(\xi_0 + h/f)^2}}{2} \tag{74}$$

$$\eta = \frac{\xi_0 + h/f}{\xi} \tag{75}$$

($2f$ is the distance between foci).

In their turn, the ξ- and η-components of the dipole momentum are

$$d_\xi = d_z \frac{\eta\sqrt{\xi^2 - 1}}{\sqrt{\xi^2 - \eta^2}} \tag{76}$$

and

$$d_\eta = d_z \frac{\xi\sqrt{1 - \eta^2}}{\sqrt{\xi^2 - \eta^2}}, \tag{77}$$

respectively.

Substituting these expressions into (42), one can find the components of the total dipole momentum, and then, by means of (18), find the radiative decay rate as a function of the displacement Δx:

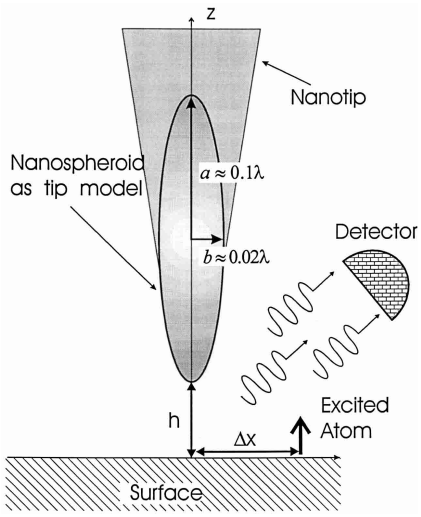

Fig. 8. Geometry of an apertureless scanning microscope with an excited atom as an object.

$$\left(\frac{\gamma}{\gamma_0}\right)^{\text{radiative}}_{\text{scan}} (\Delta x, h) = \left|1 + G_{10}\left(\frac{1}{2}\ln\left(\frac{\xi+1}{\xi-1}\right) - \frac{\xi}{\xi^2-\eta^2}\right)\right|^2 + 4|G_{11}|^2 \frac{\eta^2(1-\eta^2)}{(\xi^2-\eta^2)^2(\xi^2-1)}\cdot \tag{78}$$

Here ξ and η are described by expressions (74, 75).

Figures 9 and 10 present relationship (78) for a silver spheroid (Ag: $\varepsilon = -15.37 + \mathrm{i}0.231$, $\lambda = 632.8$ nm [44]). Figure 9 illustrates the resonance case ($\xi_0 = 1.0236$), *i.e.*, the case where condition (71) is satisfied, whereas Figure 10 shows the scanning signal for a silver spheroid of slightly different shape ($\xi_0 = 1.02$). It is seen from these figures that one can expect a substantial enhancement of the decay rates when the distance between tip of spheroid and atomic oscillator is minimal. It is interesting that in the case of small detuning (Fig. 10) the scanning signal becomes more complicated and a substantial inhibition of the decay rates is possible at $\Delta x \approx f = 0.1\lambda$. At this point the atom and the spheroid have equal dipole momenta of opposite signs. As a result, the total dipole momentum comes close to zero, and radiation is suppressed.

The central peak can be used to determine the position of the atom. In the neighbourhood of the scanning signal maximum

$$\xi^2 = \xi_0^2 + \frac{\xi_0^2}{\xi_0^2 - 1}\left(\frac{\Delta x}{f}\right)^2 \approx \xi_0^2$$
$$\eta^2 = \frac{\xi_0^2}{\xi^2} \approx 1. \tag{79}$$

Considering expressions (79), the shape of the resonance curve is governed by the resonance part of the first term

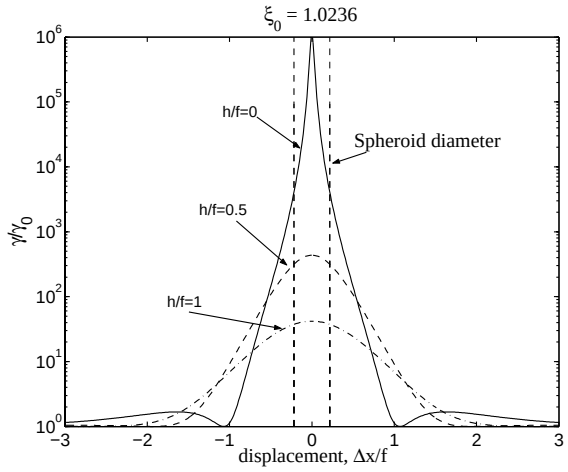

(a)

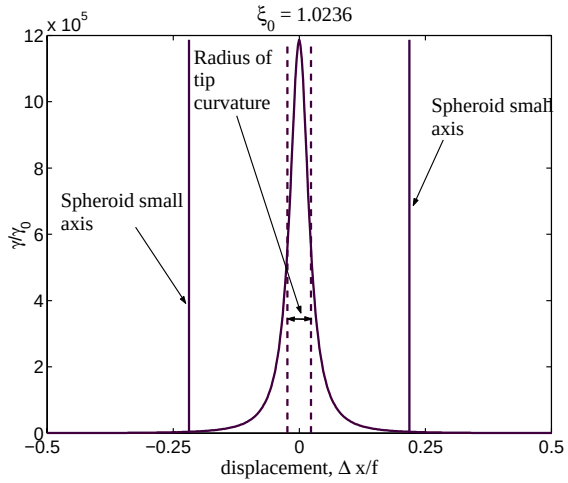

(b)

Fig. 9. Radiated power (relative radiative losses) as a function of the dipole displacement Δx relative to a silver spheroid (Ag: $\varepsilon = -15.37 + \mathrm{i}0.231$, $\lambda = 632.8$ nm) for various minimal heights h. The dipole is oriented along the z-axis, the case of plasmon resonance ($\xi_0 = 1.0236$): (a) logarithmic scale; (b) linear scale ($h = 0$).

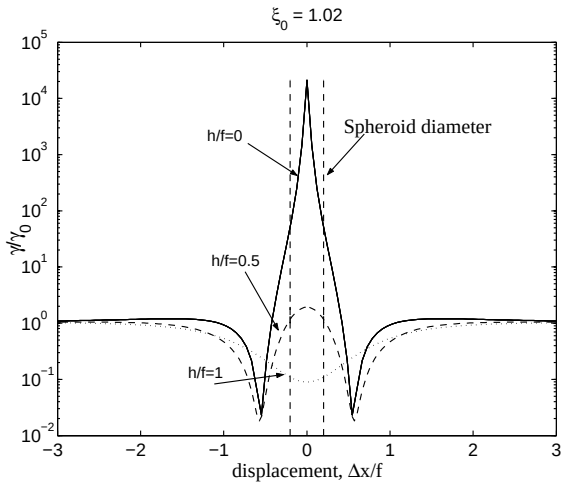

(a)

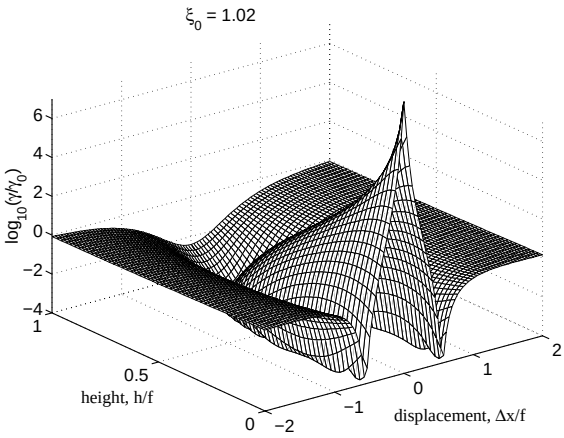

(b)

Fig. 10. Radiated power (relative radiative losses) as a function of the dipole displacement Δx relative to a silver spheroid (Ag: $\varepsilon = -15.37 + \mathrm{i}0.231$, $\lambda = 632.8$ nm) for various minimal heights h. The dipole is oriented along the z-axis: (a) the case of small detuning from resonance ($\xi_0 = 1.02$); (b) 3D view of (a).

in expression (78):

$$\left(\frac{\gamma}{\gamma_0}\right)^{\text{radiative}}_{\text{scan}} (\Delta x, h=0) \approx \left|\frac{G_{10}\xi}{\xi^2-\eta^2}\right|^2 \approx \left|\frac{G_{10}\xi_0^3}{\xi^4-\xi_0^2}\right|^2. \tag{80}$$

The contribution from the second term is strongly suppressed because of both the smallness of G_{11} and the fact that the factor $\eta^2 - 1$ tends to zero near the maximum. Substituting expression (79) into (80), we obtain the following simple asymptotic expression for the scanning signal close to the maximum:

$$\left(\frac{\gamma}{\gamma_0}\right)^{\text{radiative}}_{\text{scan}} (\Delta x, h=0) \approx \frac{f^2|G_{10}|^2}{4\left(\Delta x^2 + (R_{\text{curv}}/2)^2\right)} \tag{81}$$

where $R_{\text{curv}} = f(\xi_0^2 - 1)/\xi_0$ is the radius of curvature of the nanospheroid near its vertex (tip). One can see from the above figures that the width of the signal peak at half maximum is approximately equal to the radius of curvature of the nanospheroid near it vertex (tip). In the case under consideration (Fig. 9b), the width of the peak is about $0.044f \approx 0.0044\lambda$, that is, about 2.8 nm for $\lambda = 632.8$ nm. That is why the accuracy of determination of the atomic coordinate is about 3 nm. Besides, using a more complex scanning signal processing algorithm allowing for the drastic reduction of the decay rates at $\Delta x \approx f = 0.1\lambda$ (Fig. 10a) will make it possible to determine the position of the excited atom to an even higher precision.

5 Frequency shift in an atom placed near the tip of a prolate spheroid

Now let us consider frequency shifts in more detail. As it can be seen from the expressions (56–58), these shifts are described by double series, so that their analysis is a rather complicated matter.

In the particular but very important case of atom on the axis of a spheroid ($\eta = 1$), only the terms with $m = 0$ and 1 remain nonzero. As a result, the expressions for the frequency shifts simplify greatly in this case:

$$\left(\frac{\Delta\omega}{\gamma_0}\right)_{\xi,\eta=1} = \frac{3}{4(k_0 f)^3}\sum_{n=1}^{\infty}(2n+1)\mathrm{Re}(G_{n0})\left(\frac{\mathrm{d}}{\mathrm{d}\xi}Q_n(\xi)\right)^2, \tag{82}$$

$$\left(\frac{\Delta\omega}{\gamma_0}\right)_{\eta,\eta=1} = \left(\frac{\Delta\omega}{\gamma_0}\right)_{\psi,\eta=1} = -\frac{3}{8(k_0 f)^3} \times \sum_{n=1}^{\infty}(2n+1)G_{n1}\left(\frac{\mathrm{d}}{\mathrm{d}\xi}Q_n(\xi)\right)^2. \tag{83}$$

Another case when the expressions for the frequency shifts admit simplification, is the one when the shape of the spheroid is the spherical one ($\xi \approx R/f > \xi_0 \approx R_0/f \to \infty$). In that case, we have the following respective expressions for ξ (radial) orientation

$$\left(\frac{\omega-\omega_0}{\gamma_0}\right)_{\xi} = -\frac{3}{4}\frac{\varepsilon-1}{(k_0R)^3}\sum_{n=1}^{\infty}\frac{n(n+1)^2}{(\varepsilon+1)n+1}\left(\frac{R_0}{R}\right)^{2n+1} \tag{84}$$

and η, ψ (tangential) orientations

$$\left(\frac{\omega-\omega_0}{\gamma_0}\right)_{\eta,\psi} = -\frac{3}{8}\frac{\varepsilon-1}{(k_0R)^3}\sum_{n=1}^{\infty}\frac{n^2(n+1)}{(\varepsilon+1)n+1}\left(\frac{R_0}{R}\right)^{2n+1}. \tag{85}$$

Naturally expressions (84, 85) coincide with the corresponding expressions for a dielectric nanosphere [15], which confirms the correctness of our calculations.

In the case of highly prolate spheroid ($\xi_0 \to 1$), the main contribution is again from the terms with $m = 0$ and 1, as in the case of oscillator on the axis of the spheroid. In this case, frequency shifts are described by the following expressions ($\xi_0 \to 1$):

$$\left(\frac{\Delta\omega}{\gamma_0}\right)_{\xi} = -\frac{3}{4(k_0 f)^3}\frac{(\varepsilon-1)(\xi^2-1)(\xi_0-1)}{(\xi^2-\eta^2)} \times \sum_{n=1}^{\infty}(2n+1)\left(n(n+1)\left(\frac{\mathrm{d}}{\mathrm{d}\xi}Q_n(\xi)P_n(\eta)\right)^2 + \frac{2}{(1+\varepsilon)n(n+1)}\left(\frac{\mathrm{d}}{\mathrm{d}\xi}Q_n^1(\xi)P_n^1(\eta)\right)^2\right) \tag{86}$$

$$\left(\frac{\Delta\omega}{\gamma_0}\right)_{\eta} = -\frac{3}{4(k_0 f)^3}\frac{(\varepsilon-1)(1-\eta^2)(\xi_0-1)}{(\xi^2-\eta^2)} \times \sum_{n=1}^{\infty}(2n+1)\left(n(n+1)\left(Q_n(\xi)\frac{\mathrm{d}}{\mathrm{d}\eta}P_n(\eta)\right)^2 + \frac{2}{(1+\varepsilon)n(n+1)}\left(Q_n^1(\xi)\frac{\mathrm{d}}{\mathrm{d}\eta}P_n^1(\eta)\right)^2\right) \tag{87}$$

$$\left(\frac{\Delta\omega}{\gamma_0}\right)_{\psi} = -\frac{3}{2(k_0 f)^3}\frac{(\varepsilon-1)(\xi_0-1)}{(1+\varepsilon)(\xi^2-1)(1-\eta^2)} \times \sum_{n=1}^{\infty}\frac{(2n+1)}{n(n+1)}\left(Q_n^1(\xi)P_n^1(\eta)\right)^2. \tag{88}$$

In the limit $\eta \to 1$, these expressions agree with expressions (82, 83), taken in the limit $\xi_0 \to 1$. The most interesting feature of expressions (86–88) is that the frequency shifts tend to zero in the case of infinitely thin dielectric needle ($\xi_0 = 1$) and fixed atomic position ($\xi = const$).

In the case of ideally conducting spheroid, we have, instead of expressions (86–88)

$$\left(\frac{\Delta\omega}{\gamma_0}\right)_{\xi} = \frac{3}{2(k_0 f)^3}\frac{(\xi^2-1)}{(\xi^2-\eta^2)\ln\left(\frac{\xi_0-1}{2}\right)} \times \sum_{n=1}^{\infty}(2n+1)\left(\frac{\mathrm{d}}{\mathrm{d}\xi}Q_n(\xi)P_n(\eta)\right)^2 \tag{89}$$

$$\left(\frac{\Delta\omega}{\gamma_0}\right)_{\eta} = \frac{3}{2(k_0 f)^3}\frac{(1-\eta^2)}{(\xi^2-\eta^2)\ln\left(\frac{\xi_0-1}{2}\right)} \times \sum_{n=1}^{\infty}(2n+1)\left(Q_n(\xi)\frac{\mathrm{d}}{\mathrm{d}\eta}P_n(\eta)\right)^2 \tag{90}$$

$$\left(\frac{\Delta\omega}{\gamma_0}\right)_{\psi} = -\frac{3}{2(k_0 f)^3}\frac{(\xi_0-1)}{(\xi^2-1)(1-\eta^2)} \times \sum_{n=1}^{\infty}\frac{(2n+1)}{n(n+1)}\left(Q_n^1(\xi)P_n^1(\eta)\right)^2. \tag{91}$$

The analysis of expressions (89–91) and (86–88) shows that in the case of ideally conducting spheroid the frequency shifts of ξ- and η-oriented oscillators are greater than those occurring near a dielectric spheroid. Nevertheless, the frequency shifts tend to zero as the spheroid tapers off into a needle, $\xi_0 \to 1$. The relative frequency shifts are shown in Figures 11 and 12 as a function of the distance between the atom and the surface of the spheroid for various spheroid shapes and dipole orientations. The oscillator is located on the axis of the spheroid with $\varepsilon = 3$.

One can see from these figures that, as in the case of decay rates, the frequency shifts for an oscillator located near a needle ($\xi_0 = 1.1$) is much greater than those occurring in the same oscillator near a sphere ($\xi_0 = 10$).

The dependence of the frequency shift of an atomic dipole on its distance from the surface of a spheroid in an almost resonant case is shown in Figure 13. The most

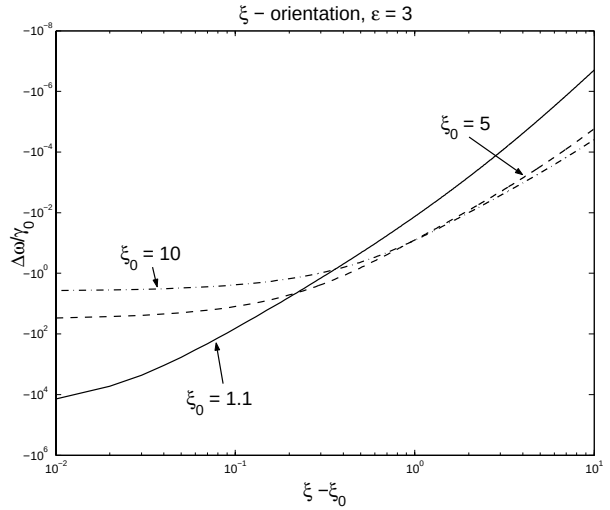

Fig. 11. Relative frequency shift $(\omega - \omega_0)/\gamma_0$ as a function of the distance of the dipole (ξ) from the surface of the spheroid and the size ξ_0 of the latter ($\varepsilon = 3$, the dipole is located on the major axis of the spheroid and oriented along it).

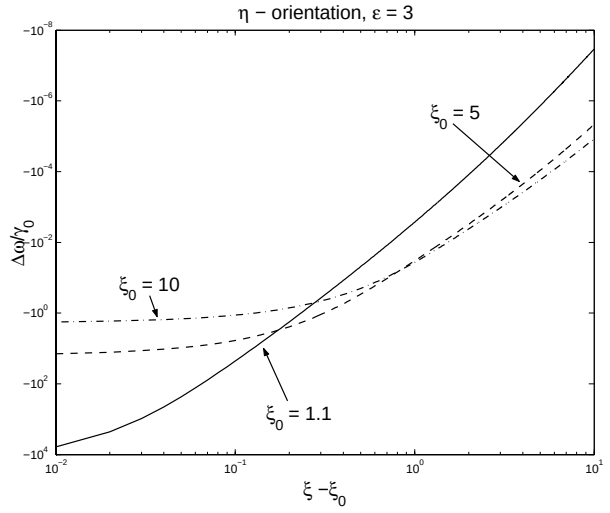

Fig. 12. Relative frequency shift $(\omega - \omega_0)/\gamma_0$ as a function of the distance of the dipole (ξ) from the surface of the spheroid and the size ξ_0 of the latter ($\varepsilon = 3$, the dipole is located on the major axis of the spheroid and oriented perpendicular to it).

noteworthy feature is the appearance of positive values of the shift. This corresponds to *repulsion* between the atom and the spheroid under conditions considered. In an ordinary situation, the van der Waals attraction predominates, and so the frequency shift is negative. A similar frequency shift behaviour has been previously predicted in other cases of resonance interaction, specifically in the case of interaction of an excited atom with the whispering gallery modes of a dielectric microsphere [15].

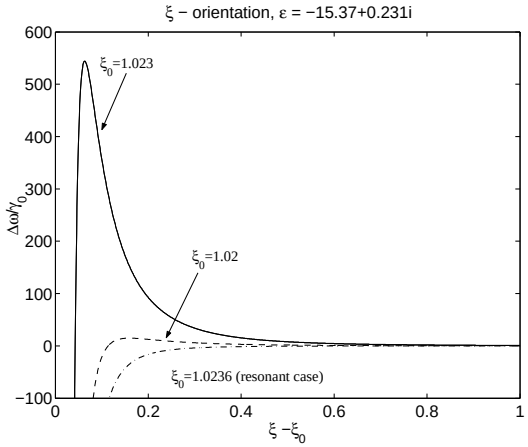

Fig. 13. Relative frequency shift of a dipole as a function of its distance from the surface of an almost resonant silver nanospheroid. The dipole is located on the major axis of the spheroid axis and oriented along it.

6 Conclusion

In this paper we have shown that a dielectric or a metallic prolate spheroid can substantially influence the decay rates and frequency shifts of an atom placed near it. Using the quasistatic approach that is valid in the case of nanobodies, we have found analytical expressions for the decay rates and frequency shifts for any oscillator position and orientation.

Spheroids occupy an intermediate position between the cylinder and the sphere, and then ellipticity can be used to effectively control the spectroscopic characteristics of atoms placed near them. Of special importance is the case when the shape of the spheroid matches with its permittivity, in such a way that a polariton resonance occurs at a frequency close to the atomic frequency. Herewith a dramatic enhancement of the decay rates takes place.

The predictions of this paper apply to any surface polariton resonances, such as the surface plasmon or surface phonon resonances in dielectric materials (sapphire) in the mid infrared [12], which have recently been shown to dramatically alter the properties of excited-state atoms (surface repulsion [47], enhancement of radiationless decay rates [48]).

The excited atomic oscillator plus prolate nanospheroid system has been used as a model of an apertureless scanning microscope. We have shown that the accuracy of determination of the position of the excited atom is substantially better than the diameter of the nanospheroid, and mainly limited by the radius of curvature of the nanospheroid vertex (tip). In a typical case, it can be of the order of 3 nm and better.

All the results obtained are valid when the spheroid size and distance between an atom and the spheroid are much smaller than the radiation wavelength. The actual scope of applicability of our results can be found once comparison is made with the solution of the fully quantum electrodynamic problem involving frequency-dependent

permittivity. This problem will be considered in a forthcoming publication.

The authors thank the Russian Foundation for Basic Research (V.K., V.L.), CENTER "Integration" (V.K.), and Centre National de la Recherche Scientifique (V.K., M.D.) for their financial support of this work. One of the authors (V.K.) thanks the Laboratoire de Physique des Lasers (Université Paris-Nord), where this work was finished, for its hospitality. We are also grateful to anonymous referee, whose comments promote the improvement of the paper.

References

1. *Near Field Optics*, edited by D.W. Pohl, D. Courjon (Kluwer Acad. Publ., Dordrecht, 1992)
2. *Near Field Nano/Atom Optics and Technology*, edited by M. Ohtsu (Springer, Berlin, 1998)
3. V.I. Balykin, V.S. Letokhov, Phys. Today **42**, 23 (1989); V.I. Balykin, V.S. Letokhov, *Atom Optics with Laser Light* (Harwood Academic Publishers, 1995)
4. P. Meystre, *Atom Optics* (Springer Verlag, Berlin, 2001)
5. E.M. Purcell, Phys. Rev. **69**, 681 (1946)
6. S. Haroche, Cavity quantum electrodynamics, in: Les Houches, Session LIII, 1990, edited by J. Dalibard, J.M. Raimond, J. Zinn-Justin, *Fundamental Systems in Quantum Optics* (North-Holland, Amsterdam, 1992)
7. *Cavity Quantum Electrodynamics*, edited by P. Berman (Academic Press, New York, 1994)
8. K.H. Drexhage, *Progress in Optics XII*, edited by E. Wolf (North-Holland, N.Y., 1974), Vol. 12, p. 165
9. W. Lucosz, R.E. Kunz, Opt. Commun. **20**, 195 (1977)
10. G. Barton, J. Phys. B **16**, 2134 (1974); M. Babiker, G. Barton, J. Phys. A **9**, 129 (1976)
11. G. Barton, Proc. R. Soc. Lond. A **453**, 2461 (1997)
12. M. Fichet, F. Schuller, D. Bloch, M. Ducloy, Phys. Rev. A **51**, 1553 (1995); M.-P. Gorza, S. Saltiel, H. Failache, M. Ducloy, Eur. Phys. J. D **15**, 113 (2001)
13. H. Chew, J. Chem. Phys. **87**, 1355 (1987)
14. V.V. Klimov, M. Ducloy, V.S. Letokhov, J. Mod. Opt. **43**, 549 (1996)
15. V.V. Klimov, M. Ducloy, V.S. Letokhov, J. Mod. Opt. **43**, 2251 (1996)
16. V.V. Klimov, M. Ducloy, V.S. Letokhov, Phys. Rev. A **59**, 2996 (1999)
17. V.B. Braginsky, V.S. Ilchenko, Dokl. SSSR **293**, 1358 (1987)
18. V.B. Braginsky, M.L. Gorodetsky, V.S. Ilchenko, Phys. Lett. A **137**, 393 (1989)
19. L. Collot, V. Lefevre-Seguin, M. Brune, J.M. Raimond, S. Haroche, Europhys. Lett. **23**, 327 (1993)
20. H. Nha, W. Jhe, Phys. Rev. A **56**, 2213 (1997)
21. J. Enderlein, Chem. Phys. Lett. **301**, 430 (1999)
22. W. Zakowicz, M. Janowicz, Phys. Rev. A **62**, 013820 (2000)
23. V.V. Klimov, M. Ducloy, Phys. Rev. A **62**, 043818 (2000)
24. V.V. Klimov, Pism. ZhETF **68**, 610 (1998)
25. V.V. Klimov, V.S. Letokhov, Phys. Rev. A **54**, 4408 (1996); V.V. Klimov, V.S. Letokhov, Opt. Commun. **122**, 155 (1996)
26. V.V. Klimov, V.S. Letokhov, Comm. At. Mol. Phys. **2**, 15 (2000)
27. V.V. Klimov, M. Ducloy, V.S. Letokhov, Kvant. Elektr. **31**, 569 (2001)
28. M.B. Mohamed, V. Volkov, S. Link, M.A. El-Sayed, Chem. Phys. Lett. **317**, 517 (2000)
29. F. Zenhausen, Y. Martin, H. Wickramasinghe, Science **269**, 1083 (1995)
30. R. Kopelman, W. Tan, Science **262**, 778 (1997)
31. S. Sekatskii, V.S. Letokhov, JETP Lett. **63**, 319 (1996); Appl. Phys. B **63**, 525 (1996)
32. J.M. Wylie, J.E. Sipe, Phys. Rev. A **30**, 1185 (1984); A **32**, 2030 (1985)
33. M.G. Belkina, Characteristics of Radiation of Prolate Ellipsoid of Revolution, in: *Diffraction of Electromagnetic Waves on Some Bodies of Revolution* (Sovetskoe Radio, Moscow, 1957), p. 126
34. V.G. Farafonov, Different. Eq. **19**, 1765 (1983)
35. S. Asano, G. Yamamoto, Appl. Opt. **14**, 29 (1975)
36. R.R. Chance, A. Prock, R. Sylbey, Adv. Chem. Phys. **37**, 1 (1978)
37. L. Knoll, S. Scheel, D.G. Welsch, `quant-ph/000621-27`
38. Ho Trung Dung, L. Knöll, D.G. Welsch, Phys. Rev. A **64** 013804 (2001)
39. A.F. Stevenson, J. Appl. Phys. **24**, 1134 (1953)
40. W. Smythe, *Static and Dynamic Electricity* (New York, Toronto London, 1950)
41. *Handbook of Mathematical Functions*, edited by M. Abramowitz, I.A. Stegun (NBS, 1964)
42. R.B. Vaganov, B.Z. Katsenelenbaum, *Fundamentals of the Diffraction Theory* (Nauka, Moscow, 1982)
43. *Surface Polaritons. Electromagnetic Waves on Surfaces and at Interfaces*, edited by V.M. Agranovich, D.L. Mills (Nauka, Moscow, 1985)
44. Q.Q. Shu, P.K. Hansma, Thin Solid Films **384**, 76 (2001)
45. G. Hass, L. Hadley, *Optical Properties of Metals*, edited by D.E. Gray, American Institute of Physics handbook (New York, McGraw-Hill, 1963), p. 6
46. V.V. Klimov, M. Ducloy, V.S. Letokhov, Chem. Phys. Lett. (in press)
47. H. Failache, S. Saltiel, M. Fichet, D. Bloch, M. Ducloy, Phys. Rev. Lett. **83**, 5467 (1999)
48. H. Failache, S. Saltiel, A. Fischer, D. Bloch, M. Ducloy, Phys. Rev. Lett. **88**, 243603 (2002)